Metastable Mesoscopic Clusters in Solutions of Sickle-Cell Hemoglobin

Weichun Pan,* Oleg Galkin,* Luis Filobelo,* Ronald L. Nagel,‡ and Peter G. Vekilov*†
*Department of Chemical Engineering and †Department of Chemistry, University of Houston, Houston, Texas 77204-4004; and ‡Division of Hematology, Department of Medicine, Albert Einstein College of Medicine, The Bronx, New York 10461

ABSTRACT Sickle cell hemoglobin (HbS) is a mutant, whose polymerization while in deoxy state in the venous circulation underlies the debilitating sickle cell anemia. It has been suggested that the nucleation of the HbS polymers occurs within clusters of dense liquid, existing in HbS solutions. We use dynamic light scattering with solutions of deoxy-HbS, and, for comparison, of oxy-HbS and oxy-normal adult hemoglobin, HbA. We show that solutions of all three Hb variants contain clusters of dense liquid, several hundred nanometers in size, which are metastable with respect to the Hb solutions. The clusters form within a few seconds after solution preparation and their sizes and numbers remain relatively steady for up to 3 h. The lower bound of the cluster lifetime is 15 ms. The clusters exist in broad temperature and Hb concentration ranges, and occupy 10^{-5}–10^{-2} of the solution volume. The results on the cluster properties can serve as test data for a potential future microscopic theory of cluster stability and kinetics. More importantly, if the clusters are a part of the nucleation mechanism of HbS polymers, the rate of HbS polymerization can be controlled by varying the cluster properties.

INTRODUCTION

Sickle cell hemoglobin (HbS) differs from the normal adult variant (HbA) by a mutation from glutamate to valine at the sixth site of its two β-chains (1–3) (a model of a HbA molecule in shown in Fig. 1 *a* (4)). This mutation allows hydrophobic contacts between valine of one Hb molecule and alanine, phenylalanine, and leucine from other HbS molecules and the formation of a twisted 14-member polymer fiber (5–8). Multiple polymers interacting in solution behave as a gel-like phase (9). HbS polymerization and gelation, which occur when HbS is in deoxy-state in the venous circulation, are considered the primary pathogenic event of sickle cell anemia (10–15). Hence, the thermodynamics of HbS solutions (16–25) and the formation of the polymers and of other condensed phases (9,26–31) are studied as part of the fundamental mechanisms of the disease. These investigations have revealed that over periods of several days, HbS solutions form crystals (32–34). The polymers are metastable with respect to the crystals and are experimentally observable because of the slow kinetics of crystal formation. It was also shown that dense liquid only forms in HbS solutions if the attraction between the molecules is enhanced by addition of polyethylene glycol or high-concentration phosphate (30,35–37).

Recently, there has been an extensive discussion of a nucleation mechanism for ordered solids (of which HbS polymers are an example), whereby dense liquid phases serve as precursors and enhancers of nucleation (30,38–45). In view of the lack of macroscopic dense liquid in near physiological HbS solutions, particularly important is the finding that such dense liquids participate in the nucleation mechanism even if they are metastable with respect to the generating solution and only exist as mesoscopic clusters (41,44,45). In this article, we test if such metastable clusters of dense liquid exist in solutions of deoxy-HbS and, for comparison, in solution of oxy-HbS and oxy-normal adult hemoglobin, HbA. We probe if the cluster lifetimes are limited and monitor the variations of the sizes and the numbers of the clusters as functions of temperature and hemoglobin concentration. As a measure of cluster stability, we estimate the fraction of the total solution volume occupied by the clusters.

METHODS

Solutions

Details of solution preparation procedures are described in Galkin and Vekilov (31); here we only summarize the main stages. Hemoglobin S and A were prepared by lysis of red blood cells from blood donated by sickle cell patients or healthy donors, respectively, following National Institutes of Health regulations and procedures approved by the University of Houston. HbS and A were purified by fast protein liquid chromatography. After purification, buffer exchange, and concentration, the stock solutions were exposed to carbon monoxide and stored in liquid nitrogen. Before an experiment, a 20 μl sample of the stock solution was placed in a glove box filled with argon to remove the bound carbon monoxide. To prepare oxy-HbS and A solutions, solution samples was exposed to air. To prepare deoxy-HbS solution, sodium dithionite was added to a final concentration of 0.055 M to maintain a reductive environment around the HbS molecules. The quality of the hemoglobin in the solution sample was checked by recording a spectrum in the slide in the 450–750 nm wavelength range. Experiments were performed with HbS solutions in 0.15 M potassium phosphate buffer with pH = 7.35. The final concentration of HbS was determined using Drabkin reagent.

Light scattering

Light scattering data were collected with an ALV goniometer equipped with He-Ne laser (632.8 nm) and ALV-5000/EPP Multiple tau Digital Correlator (ALV-GmbH, Langen, Germany). The typical cuvettes for light scattering are cylindrical with a 10 mm diameter. These cuvettes require at least 400 μl of solution. We fabricated small-volume cuvettes from a silica tube with an

Submitted August 7, 2006, and accepted for publication September 21, 2006.
Address reprint requests to Peter G. Vekilov, E-mail: vekilov@uh.edu.

0006-3495/07/01/267/11 $2.00
doi: 10.1529/biophysj.106.094854

inside diameter of 1.5 mm, which require ~30 μl solution samples. The results obtained with the small cuvettes were validated by comparison to data acquired using a standard cuvette with the more readily available HbA. Before loading in the cuvette, the solutions were filtered through 0.22 μm Millipore filters. For experiments with deoxy-HbS, the small cuvettes were sealed with cement from Mount Quick (Daido Sangyo, Japan), which is impermeable to oxygen. Intensity correlation functions were acquired at 90° for 60 s. In some cases, for comparison, correlation functions were acquired at 30° and 60°.

Determinations of cluster sizes by dynamic light scattering

The intensity correlation function $g_2(\tau)$ characterizes the rate of intensity variations $I(t)$ over a total acquisition time Δt. g_2 is defined from the intensity at two times, t and $t - \tau$ as (46)

$$g_2(\tau) = \langle I(t)I(t-\tau)\rangle_{\Delta t}/\langle I\rangle^2_{\Delta t}, \quad (1)$$

where $\langle\ \rangle_{\Delta t}$ signifies averaging over time Δt and $\langle I\rangle_{\Delta t}$ is the average intensity for the entire period of data acquisition. Since light is scattered by the fluctuations of concentration, the correlation function mostly characterizes the rate of diffusion of the scatterers during the decay of the fluctuations (47). This diffusion rate is, in turn, determined by scatterers' sizes and the viscosity of the medium, in which they are suspended (48).

The normalized correlation function $g_2(\tau)$, illustrated in Fig. 1 *b*, can be represented as the square of the sum of exponential members, each corresponding to a population of scatterers with a diffusion rate Γ_i. The noise in the signal is represented as an extra additive ε. Our dynamic light scattering experiments are aimed at identifying one or two scatterers: single Hb molecules and, in some cases, larger clusters. Hence (49)

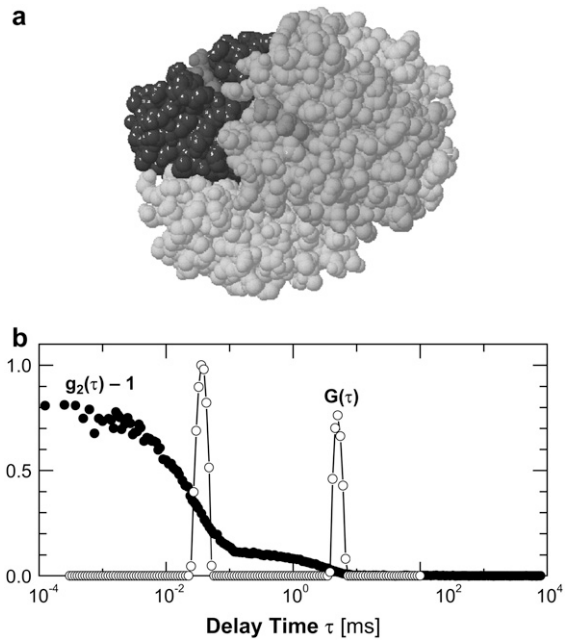

FIGURE 1 (*a*) Model of HbA (4). Turquoise and ochre mark two β-chains, cobalt and green mark two α-chains. Red and blue mark two (out of four) hemes visible in this view. Long molecular dimension is ~5.5 nm, molecular mass $M_w = 64{,}000$ g mol^{-1}. (*b*) Light scattering characterization of solutions of sickle-cell hemoglobin in deoxy-state (deoxy-HbS). Examples of the correlation function $g_2(\tau)$ (solid circles) and the corresponding delay time distribution function $G(\tau)$ (open circles) of a deoxy-HbS solution with $C_{Hb} = 67$ mg ml^{-1} at $T = 25$°C.

$$g_2(\tau) - 1 = \left(A_1 e^{-\tau/\tau_1} + A_2 e^{-\tau/\tau_2}\right)^2 + \varepsilon(0, \sigma(\tau)), \quad (2)$$

where $\tau_1 = 1/\Gamma_1$ and $\tau_2 = 1/\Gamma_2$ are the characteristic times of the diffusion of scatterers (Γ_1 and Γ_2 are the respective diffusion rates), whose contribution to the scattered light has amplitudes A_1 and A_2. $\varepsilon(0,\sigma(\tau))$ is the noise function, which is expected to have a Gaussian distribution with width σ, centered at 0.

The characteristic times τ_1 and τ_2 are more readily determined from the distribution function of the decay rates $G(\tau)$, illustrated in the same Fig. 1 *b*. This $G(\tau)$ can be expressed as

$$g_2(t) - 1 = \left(\int G(\tau)\exp(-t/\tau)d\tau\right)^2, \quad (3)$$

and is calculated by numerically inverting the Laplace transform with $(g_2 - 1)^{1/2}$, using a software package from ALV-Gmbh based on the CONTIN algorithm (50,51).

To calculate the equivalent hydrodynamic radii for the values of relaxation times $\tau_1 = 37$ μs for the HbS molecules and $\tau_2 = 5.04$ ms for the clusters in Fig. 1 *b*, we use the Stokes-Einstein relation, modified with $\Gamma_i = \tau_i^{-1} = D_i q^2$:

$$R_i = \frac{k_B T q^2}{6\pi\eta_i}\tau_i, \quad (4)$$

where $i = 1, 2$ for single molecules or clusters, respectively, k_B is the Boltzmann constant, T is absolute temperature, η_i is the viscosity to which a diffusing object i is exposed, and D_i is its diffusion coefficient. In our experiments $\lambda = 632.8$ nm (He-Ne laser), the refractive index $n = 1.33$ (water), and $\theta = 90°$, so that the scattering vector $q = 4\pi n/\lambda \sin(\theta/2) = 18.7 \times 10^4$ cm^{-1}. For the HbS molecules, we take the viscosity to be that of 0.15 M potassium phosphate buffer, $\eta_1 = \eta|_{T\,=\,20°C} = 1.057$ cP (52), and assuming temperature dependence similar to water, $\eta|_{T\,=\,25°C} = 0.937$ cP. Then $R_1 = 3.01$ nm, which is in acceptable agreement with the known diameter of the Hb molecule of 5.5 nm. Because the sizes of clusters are significantly greater than the size of the HbS molecules, in calculations for the clusters we use the viscosity of the HbS solution (53) (we assume that the cluster presence does not affect the viscosity, which is reasonable because of their low volume fraction)

$$\eta_2 = \eta_{HbS} = \eta_0 \exp\left(\frac{[\eta]C}{1 - \frac{k}{\nu}[\eta]C}\right), \quad (5)$$

where $\eta_0 = \eta_1$ is the viscosity of the buffer, $[\eta] = 0.036$ dl/g is the viscosity increment, C is the concentration of Hb in $g\ dl^{-1}$, k is a ''crowding factor,'' ν is a shape coefficient for nonspherical particles so that $k/\nu = 0.42$ (53). For $C = 67$ mg ml^{-1}, $\eta_2 = 1.226$ cP, and $R_2 = 313$ nm.

Determination of cluster number density and volume fractions

To estimate the concentration of clusters, we use that the ratio of the amplitudes A_1 and A_2 in Eq. (2) is (54,55)

$$\frac{A_2}{A_1} = \frac{C_2 I_2(M_2, \theta)}{C_1 I_1(M_1, \theta)}, \quad (6)$$

where C_i is the concentration of each scatterer in mg ml^{-1}, $I_i(M_i,\theta)$ is the intensity scattered at angle θ by scatterer i per unit concentration of i; M_i is the molecular weight of scatterer i. The concentration C_i is related to number density n_i as $C_i = \frac{M_i n_i}{N_A}$, where N_A is Avogadro's number.

The intensity I_1 of light scattered by HbS molecules can be obtained from the expression for the Rayleigh ratio $R_{\theta,1}$ of the scattered I_1 to incident I_0 intensity for small interacting molecules (46):

$$\frac{H_1 C_1}{R_{\theta,1}} = \frac{1}{M_1} f(C_1), \quad (7)$$

where $H_i = [(2\pi n/N_A\lambda^4)(\partial n/\partial C_i)_{T,\mu}]^2$is an instrument parameter, and $(\partial n/\partial C_i)_{T,\mu}$is the refractive index increment at constant temperature T and constant chemical potential of the remaining species μ. $f(C_1) = 1+M_1(2\tilde{B}C_1+3\tilde{C}C_1^2+4\tilde{D}C_1^3+\ldots)$ is a virial expansion with coefficients $\tilde{B},\tilde{C},\tilde{D},\ldots$. For hemoglobin we use the known values of the virial coefficients (17) $\tilde{B} = (8V_1/2M_1)$, $\tilde{C} = (15V_1^2/3/2M_1)$, $\tilde{D} = (24.48V_1^3/4/3M_1)$, $\tilde{E} = (35.3V_1^4/5/4M_1)$, $\tilde{F} = (47.4V_1^5/6/5M_1)$, $\tilde{G} = (65.9V_1^6/7/6M_1)$, where $V_1 = 0.79$ cm^3 g^{-1} is the specific volume of hemoglobin molecules (17,34,56).

For the clusters, we apply the analog of Eq. 7 for large noninteracting particles, since we anticipate the concentration of clusters to be small

$$\frac{H_2C_2}{R_{\theta,2}} = \frac{1}{M_2P(qR_2)}, \tag{8}$$

where $P(qR_2)$ is the shape factor of the clusters and R_2 is their radius. Inserting Eqs. 7 and 8 into Eq. 6 we get

$$\frac{A_2}{A_1} = \frac{C_2}{C_1}\frac{H_2}{H_1}\frac{M_2}{M_1}P(qR_2)f(C_1) \tag{9}$$

or, with the expressions for C_i and H_i,

$$\frac{n_2}{n_1} = \frac{A_2}{A_1}\frac{1}{\tilde{N}^2P(qR_2)f(C_1)}\frac{(\partial n/\partial C_2)_{T,\mu}}{(\partial n/\partial C_1)_{T,\mu}} \tag{10}$$

where $\tilde{N} = \frac{M_2}{M_1}$ is the mean number of HbS molecules in the clusters.

Taking into account $\varphi_i = n_i\frac{4}{3}\pi R_i^3$, for the volume fraction of clusters ϕ_2, we get

$$\varphi_2 = \frac{n_2}{n_1}\frac{R_2^3}{R_1^3}\varphi_1. \tag{11}$$

Introducing the protein densities ρ_1 and ρ_2 in single Hb molecules and clusters, respectively, and using $M_i = \rho_i\frac{4}{3}\pi R_i^3$we get $\tilde{N} = (\rho_2R_2^3/\rho_1R_1^3)$. Finally,

$$n_2 = \frac{A_2}{A_1}\frac{1}{P(qR_2)f(C_1)}\frac{(\partial n/\partial C_2)_{T,\mu}}{(\partial n/\partial C_1)_{T,\mu}}\left(\frac{\rho_1}{\rho_2}\right)^2\left(\frac{R_1}{R_2}\right)^6 n_1$$

$$\varphi_2 = \frac{A_2}{A_1}\frac{1}{P(qR_2)f(C_1)}\frac{(\partial n/\partial C_2)_{T,\mu}}{(\partial n/\partial C_1)_{T,\mu}}\left(\frac{\rho_1}{\rho_2}\right)^2\left(\frac{R_1}{R_2}\right)^3\varphi_1. \tag{12}$$

Assuming spherical shape of the clusters,

$$P(qR_2) = \left[\frac{3}{(qR_2)^3}(\sin(qR_2) - qR_2\cos(qR_2))\right]^2. \tag{13}$$

Since the evaluations of n_2 and ϕ_2 rely on the experimentally determined R_2 and A_2, they are affected by the errors in both determinations, and are less accurate than the evaluation of R_2. Thus, 10% uncertainties in R_2 and A_2 would result in 70% uncertainty in n_2 and 30% in ϕ_2.

To illustrate the evaluation of the cluster number density using Eq. 10, we take the ratio of the peak areas from Fig. 1 *b*: $A_1/A_2 = 64\%/36\% = 1.78$. Most measurements of the refractive index increments ∂n/∂C for different proteins fall in the range 0.1–0.2 (57), so it is safe to assume that the ratio of the increments in Eqs. 10 and 12 is of order of unity. For $C_1 = 67$ mg ml^{-1}, $f(C_1) = 1.522$. $P(qR_2) = P(5.85) = 7.37\times10^{-3}$ and we get

$$\frac{n_2}{n_1} \approx \frac{50}{\tilde{N}^2}. \tag{14}$$

To evaluate $\tilde{N}$, we first assume that the density of clusters ρ_2 is the same as that of Hb monomers ρ_1, i.e., $\rho_2 = \rho_1 = 1/V_1 = 1266$ mg ml^{-1}, which is an overestimation. With this, $\tilde{N} = (R_2/R_1)^3 \approx 10^6$, and we get $n_2/n_1 \approx 0.5\times10^{-10}$ and $\phi_2 = 0.5\times10^{-4}\phi_1$. Estimates with more realistic values for ρ_2, between 100 and 500 mg ml^{-1}, in Table 1, yield results of the same order of magnitude.

In Results below, we use $\rho_2 = 400$ mg ml^{-1} to evaluate n_2 and ϕ_2.

TABLE 1 Estimates of the number density of clusters n_2, and volume fraction occupied by clusters ϕ_2 stemming from the data in Fig. 1 for HbS concentration $C_{HbS} = 67$ mg ml^{-1}, $n_1 = C_{HbS}\,N_A/M_w = 6.3\times10^{17}$ cm^{-3}, and $\phi_1 = V_1\,C_{HbS} = 0.053$

ρ_2 [mg ml^{-1}]	100	200	300	400	500	$\rho_1 = \rho_2$
$\tilde{N}$, 10^6	0.12	0.24	0.36	0.48	0.6	1
n_2/n_1, 10^{-10}	34.8	8.8	3.9	2.2	1.4	0.5
ϕ_2/ϕ_1, 10^{-4}	34.8	8.8	3.9	2.2	1.4	0.5

In the calculation, Eqs. 10 and 12 were used assuming that in the clusters, the mass density of HbS ρ_2 and the respective number of HbS molecules $\tilde{N}$ are as shown in rows 1 and 2, and that $R_2/R_1 = 100$.

Analyses of errors in determination of cluster sizes and number densities

A general discussion of errors in dynamic light scattering can be found in Schatzel (49) and Peters (58). Here we analyze the levels of noise in our setup and the errors in the characterization of concentrated hemoglobin solutions used in this work.

The ALV-5000 digital correlator that we use captures τ values ranging from 125 ns to several hours. An important feature of this device is the use of a ''multiple-tau'' correlation technique, in which the correlation function is simultaneously calculated with a set of several different lag times τ. In contrast to systems with constant sampling times, this technique produces noise amplitude, which diminishes with increasing τ values. This is important for measurements at long lag times.

Fig. 2 *a* shows two typical examples of the correlation function at two concentrations of HbA. Because of weaker scattering at the lower HbA concentration, the respective $g_2(\tau) - 1$ apparently has higher levels of noise. To quantify this noise, we calculate the respective $G(\tau)$, determine τ_1 and τ_2, and compose two ideal $g_2(\tau)$ using Eq. 2 with $\varepsilon = 0$. The difference between the real $g_2(\tau)$ dependencies and the ideal ones is the noise function ε, plotted in the inset of Fig. 2 *a*. This noise plot shows that the mean value of the noise amplitude decreases from the ~1% of $g_2(\tau)$ at $\tau = 1$ μs to 0.01% at $\tau = 1$ s at the higher $C_{HbA} = 108$ mg ml^{-1} and from ~10% to ~0.03% at $C_{HbA} = 1$ mg ml^{-1}.

To understand the effects of such levels of noise on the accuracy of the determination of the characteristic times τ_1 and τ_2, we simulated a correlation function with noise ε. For each τ, ε was created by a random-number generator. The width of the noise distribution σ was set to decrease with increasing lag time τ as

$$\sigma = 10^a\,\tau^b. \tag{15}$$

This dependence corresponds to the linear fits in the inset of Fig. 2 *a*. The noise function $\varepsilon(\tau)$ with parameters a and b as for $C_{HbA} = 108$ mg ml^{-1} in Fig. 2 *a* is shown in Fig. 2 *b*. A simulated correlation function with a single τ_1 and this $\varepsilon(\tau)$ is shown in the same figure.

Exploring the effect on $G(\tau)$ of increasing noise levels imposed on a correlation function composed of a single exponent, we found that the width of the decay rate distribution function increases with increasing levels of noise. Although the input contains a single decay rate, addition of noise makes it similar to a distribution with multiple decay rates. Still, the position of the peak, and correspondingly, the determination of τ_1, is only weakly affected by the noise.

Correlation functions for two processes with a sufficiently large difference in decay time, which may correspond to protein molecules in solutions and their larger clusters, are of particular interest. The corresponding decay rate distribution functions $G(\tau)$ consist of two well-separated peaks. First, we probe the effects of randomly varying noise on the position of the second peak τ_2. The simulated correlation functions mimic the experimental ones: delay times $\tau_1 = 38$ ns and $\tau_2 = 3.3$ ms, ratio of amplitudes $A_1/A_2 \approx 96{:}4$, noise parameters $a = -3.2$, $b = -0.35$. Comparison of the positions of the

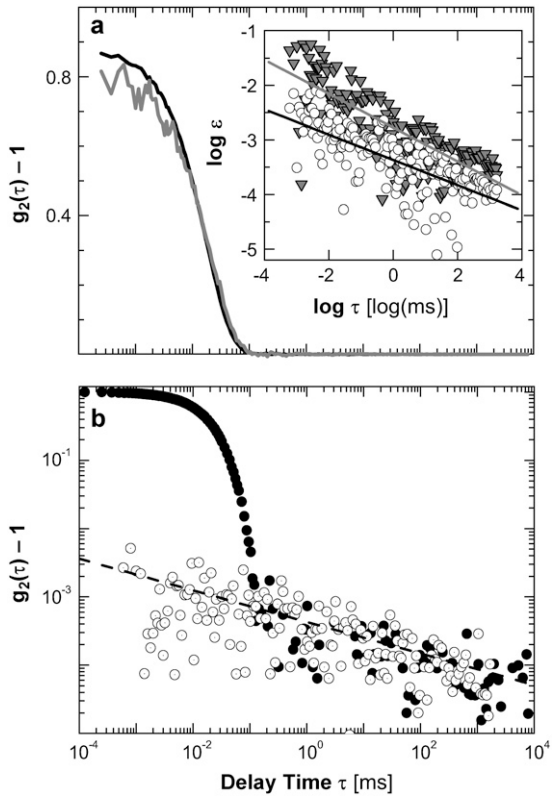

FIGURE 2 Characterization of the noise in correlation functions of dynamic light scattering intensity recorded in solutions of normal adult hemoglobin in oxy-state (oxy-HbA). (*a*) Intensity correlation functions of two solutions. Solid line, $C_{HbA} = 108$ mg/ml, corresponding mean count rate CR = 158 kHz; shaded line, $C_{Hb} = 1$ mg/ml, corresponding mean count rate CR = 15 kHz. (*Inset*) Noise level at the above conditions: open symbols, $C_{Hb} = 108$ mg/ml; solid symbols, $C_{Hb} = 1$ mg/ml; lines are respective linear fits. Data acquisition time was 30 s. (*b*) Simulated correlation function with single decay time $\tau = 0.038$ ms (*solid circles*). Open circles, simulated noise, see text; dashed line, its linear fit.

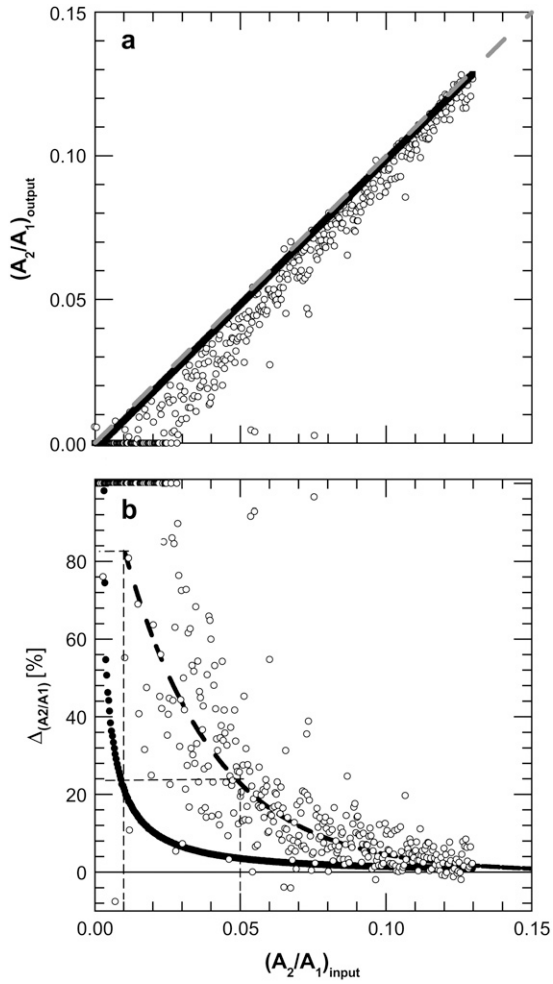

FIGURE 3 Dependence of the ratio of amplitudes of two peaks A_2/A_1, determined from simulated correlation functions, consisting of two exponential decays, on the input ratio of these amplitudes. Solid symbols (they appear as *thick solid line*), simulation with no added noise; open symbols, noise parameters $a = -3.2$, $b = -0.35$. (*a*) Absolute values of the ratio. Dashed line, ideal situation $(A_2/A_1)_{output} = (A_2/A_1)_{input}$. (*b*) Relative deviation from exact values. Dashed line, average error in the presence of noise. Thin vertical and horizontal dashed lines show that if $(A_2/A_1)_{input} > 0.05$, the error in $(A_2/A_1)_{output} < 20\%$; if $(A_2/A_1)_{input} \approx 0.01$, the $(A_2/A_1)_{output}$ error $\approx 80\%$.

two peaks, extracted from multiple repetition of data collection with HbS and from simulation with randomly varying noise, shows that the variation in the position of the second peak in the experiments is comparable to the variations in the simulations. Comparison of simulated correlation functions with the experimental ones displays that they are similar and produce similar decay rate distributions $G(\tau)$. We conclude that the variations in the experimental trace reflect the influence of the noise and not variation of sizes of the clusters.

Next, we probe how the ratio of the amplitudes of the two peaks A_2/A_1 influences the accuracy of determination of the peaks' positions and amplitudes. Simulations were performed with a set of 400 correlation functions, in which the ratio A_2/A_1 was varied linearly from 0 to 0.13. Fig. 3 shows the output amplitude ratio A_2/A_1 as a function of this ratio in the simulated correlation function and the deviation of the output from the input ratio $\Delta_{A2/A1} = \{[(A_2/A_1)_{input} - (A_2/A_1)_{output}]/(A_2/A_1)_{input}\} \times 100\%$. Fig. 3 shows that without noise, the ratio A_2/A_1 has significant error only for very small values of A_2. The error in the absence of noise is due to known inaccuracies of the numerical inversion of the Laplace transform (59). The addition of noise exacerbates the situation by increasing the error severalfold. Still, if $A_2/A_1 > 0.05$, the error in determination of this ratio is $<20\%$.

The Laplace transform inversion and the noise also affect the determined positions of the maxima of the distribution function $G(\tau)$. Without noise, the position of the first maximum is determined quite accurately, with an error of $<0.2\%$, and even with noise, the error level is 1–2%. The position of the second peak, Fig. 4, *a* and *b*, is determined with significantly lower accuracy if the amplitude A_2 is small. Fig. 4 *b* shows that at $A_2/A_1 = 0.05$, the error in the determination of the position of the second peak is between 10 percent and several tens of percent, depending on the noise level.

Finally, we consider the increase of the width of the two peaks as a result of the inaccuracy of the Laplace transform inversion and the effects of noise. Fig. 5 shows that narrow input peaks corresponding to a population of identical scatterers appear significantly wider. Again the effects are much stronger for the second peak, where the input of 3.3 ms produces a range from 2.4 to 5 ms at $(A_2/A_1)_{input} = 0.05$. This widening influences the accuracy of the determination of the peak position as discussed above.

The above estimates allow evaluation of dynamic light scattering data, in which the second peak corresponds to clusters freely diffusing in the solution. The simulation results reveal that the second peak will be undetectable if it is below the noise level. If the second peak has an amplitude higher than

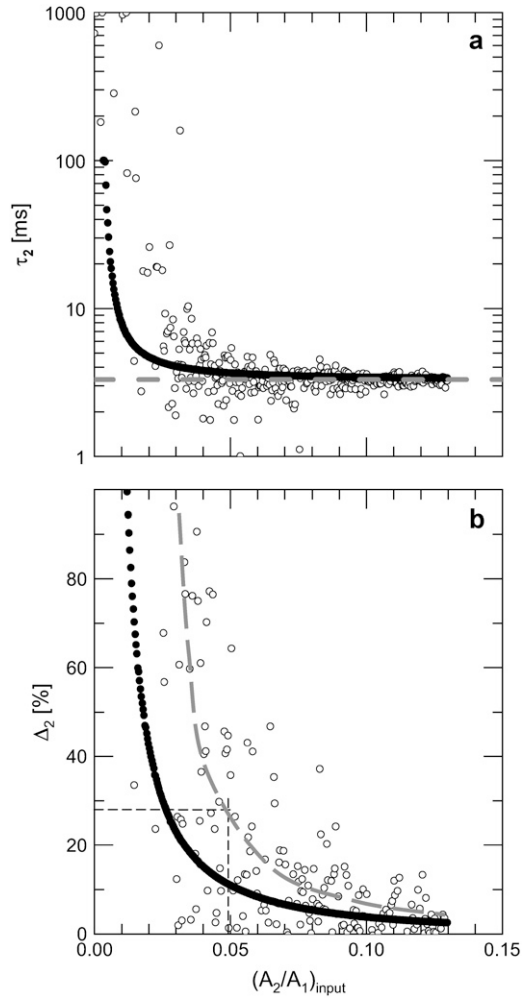

FIGURE 4 Accuracy of peak position as a function of size of second peak. (*a*) Position of second peak τ_2 peak. (*b*) Deviation of second peak from exact position in percent. Solid symbols, simulations without noise; open symbols, with noise. Shaded dashed line, position of the peak in input correlation function. Thin vertical and horizontal dashed lines in *d* show that if $(A_2/A_1)_{input} > 0.05$, the error in $\tau_2/\tau_1 < 30\%$.

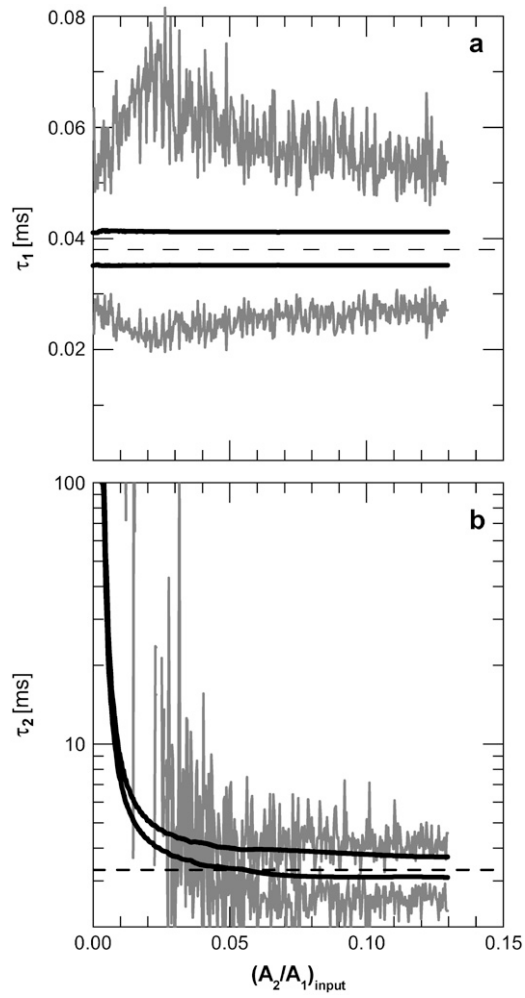

FIGURE 5 Widening of the peaks in the distribution function $G(\tau)$. Dashed line, position of peaks as input in simulations. Solid lines, range of position of output peaks with no added noise; shaded line, with noise as in Fig. 2.

this threshold, it is readily detected, but the error in the peak position is high. As the amplitude of the second peak grows, the error in the determination of its position decreases. For the characterization of solutions of HbA and HbS with concentration from 50 to 150 mg $ml^{-1,}$ for which the noise level is as discussed above, the threshold of detection of the second peak is $A_2/A_1 \approx 0.01$. The position of the second peak can be determined with an error of $<40\%$ if $A_2/A_1 \approx 0.05$ and the error drops to $\sim 10\%$ if $A_2/A_1 \approx 0.1$. The noise level can be lowered by increasing the total time of acquisition of the intensity variation trace, and by increasing the concentration of scattering molecules.

Determination of solution viscosity at low shear rates

Typical flow-through or dropping-ball viscometers require large amounts of solution and are inapplicable to tests with poorly available HbS. These viscometers operate at high shear rates, where potential weakly bound structures are likely destroyed. We developed an alternative method based on dynamic slight scattering from polystyrene beads suspended in the protein solution (60).

Noninteracting spherical particles of 390 nm size are mixed with the protein solution, and the correlation function $g_2(\tau)$ form this suspension is recoded. From $g_2(\tau)$ and the respective $G(\tau)$, we determine the decay rate Γ_2 of the beads as discussed above. Using the Einstein-Stokes equation, the viscosity η of the solution is obtained from Γ_2 as

$$\eta = \frac{k_B T}{6\pi R_o} \frac{q^2}{\Gamma_2}, \tag{16}$$

where R_o is the radius of the beads.

A diffusing particle of 0.39 μm size covers its own diameter for ~ 0.1 s. The thickness δ of the viscous boundary layer around it, at the top of which the solution velocity u vanishes, is of the order of 10 μm. The shear $s = \Delta u/\delta$ induced by the Brownian motion of such a particle is $<1\ s^{-1}$.

To verify the reliability and reproducibility of the viscosity determination procedure, we applied it to solvents with well-characterized properties using both standard and custom made small-volume cuvettes, with temperature controlled and stabilized to within 0.1°C. With deionized water and a 70% glycerol-water mixture, for which the viscosity reaches 20 cP at 15°C, the

deviation of our determinations from published data (61) was below 3% at five tested temperatures in the range 15–50°C. Tests with the protein lysozyme at 269 mg ml^{-1}, in which temperature was raised and then lowered, revealed that there is no aggregation of protein or beads during the course of the experiment, which would have been reflected in decreasing decay rates Γ_2 and increasing viscosity values.

We verified that the results with the above lysozyme solution were independent both of particle size and of the surface chemistry of the particles. For these tests, we used two new types of polystyrene beads: 1), uncoated, with a diameter of 1000 nm, or 2), with carboxylate-modified surface and diameter of 390 nm. The viscosities obtained with both new types of beads were identical to those determined using the 390 nm uncoated beads. All viscosity determinations with hemoglobin were carried out with 390 nm carboxylate-modified beads.

RESULTS

Dense liquid clusters in solutions of deoxy-HbS, oxy-HbS, and oxy-HbA

Fig. 1 *b* shows typical correlation and distribution functions $g_2(\tau)$ and $G(\tau)$ of solutions of deoxy-HbS, in which at concentration above 170 mg ml^{-1} at temperatures around 35°C polymers form. For comparison, in Fig. 6 we show typical $g_2(\tau)$ and $G(\tau)$ functions for solutions of oxy-HbS and oxy-HbA. Oxy-HbS differs from deoxy-HbS by a conformation change from T- (in deoxy-HbS) to R- (in oxy-HbS) state, which facilitates the binding of four O_2 molecules (62). Oxy-HbA differs from oxy-HbS by having a glutamate instead of valine at the two $\beta 6$ sites. The only condensed phases known for oxy-HbS and oxy-HbA are crystals that form over many days. The data in Figs. 1 *b* and 6 show that at the probed temperatures and concentrations solutions of all three proteins exhibit two processes. The first one, represented by the first peak in $G(\tau)$, has a characteristics time $\tau_1 \approx 40$ ns. If this process is diffusion of a scatterer, according to Eq. 4, its radius would be 3.03 nm. This is very close to the radius of the Hb molecule, Fig. 1 *a*, and we conclude that the first peak for all three variants reflects the diffusion of Hb molecules. The peak assigned to single oxy-HbA molecules in Fig. 6 *b* is wider, likely due to the high protein concentration in the probed sample, leading to protein interactions.

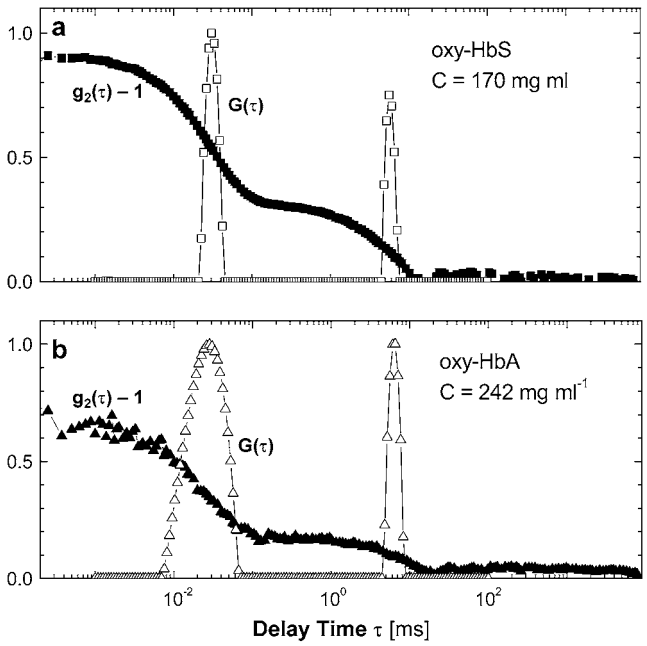

FIGURE 6 Light scattering characterization of solutions of sickle-cell hemoglobin at 35°C in oxy-state (oxy-HbS) in *a* and normal adult hemoglobin in oxy-state (oxy-HbA) in *b*; concentrations are shown in the plots. Examples of correlation function (*solid symbols*) and the corresponding delay time distribution function (*open symbols*) are shown.

The second process in Figs. 1 *b* and 6, represented by the second peaks in $G(\tau)$, is significantly slower. The amplitudes A_2 of the second peak are comparable to the amplitudes A_1 of the first peak. This allows accurate characterization of the nature of the slow process. The slow process could be not free Brownian motion of large scatterers, but diffusion of single protein molecules within immobile structures. This diffusion would be slow due to high effective viscosity. These structures would occupy part of the volume, so that single molecules in a solution of ''normal'' viscosity could still contribute to the signal; i.e., they could be either large clusters, greater than the several microns range detectable by lights scattering, or lose networks.

To test for large dense clusters of protein molecules, solution samples of the three Hb variants with Hb concentration in the range 50–450 mg ml^{-1} were loaded in 10–40 μm thick slides (30,31). (In deoxy-HbS solutions at $C_{HbS} >$ 170 mg ml^{-1}, the observation time was limited by the formation of polymers.) The slides were kept at temperatures ranging from 40°C (determined by the protein stability to denaturation) down to −5°C (below which the solution freezes) and monitored with differential interference contrast optics, sensitive to any heterogeneity larger than ~1 μm. We found no evidence of clusters or droplets larger than the detection size. Clusters of diameter < 1 μm would have characteristic diffusion time of <7 ms, and their diffusion would be reflected in Figs. 1 *b* and 6. We conclude that no large clusters or droplets exist and the second peak does not reflect diffusion within them.

Loose networks of molecules could have low refractive index and be optically undetectable. However, such networks would increase the low-shear viscosity of the protein solution, and they would be destroyed by high-shear flow. The latter consideration allows tests for the presence of loose networks by determination of the low-shear viscosity of lumazine synthase solutions. The found low-shear viscosity of the oxy-HbA and deoxy-HbS solutions was in the range 2–4 cP, equal to the high-shear values in Ross and Minton (53). The equality of the low and high shear viscosity reveals that no networks of molecules exist in these solutions and the slow process in Figs. 1 *b* and 6 is in fact diffusion of clusters of molecules of the respective Hb variant.

In Fig. 7, we monitor the time evolution of the cluster radii R_2, determined from the characteristic lag time τ_2 of the slow peak using Eq. 4 (see Methods). With all three Hb variants and at all concentrations probed, the clusters are present immediately after solution preparation. The apparent fluctuations in the R_2s at $C_{\text{deoxy-HbS}} = 67$ mg ml^{-1}, $C_{\text{oxy-HbS}} = 108$ mg ml^{-1}, and $C_{\text{oxy-HbA}} = 51$ mg ml^{-1} are likely due to random noise in the dynamic light scattering signal, analyzed in Methods above. Since the noise level decreases when the signal is stronger at higher Hb concentrations, the fluctuations in the traces with $C_{\text{deoxy-HbS}} = 131$ mg ml^{-1} and $C_{\text{oxy-HbA}} = 150$ mg ml^{-1} are weaker. Significantly, regardless of the fluctuations, the mean radii of the clusters of the three Hb variants at all probed concentrations do not increase over the 3 h of monitoring.

The cluster lifetimes

The data in Fig. 7 do not allow determination of the cluster lifetimes. In fact, if the clusters have a limited lifetime, it is possible that the slow process reflected by the correlation functions in Figs. 1 *b* and 6 is not the diffusion of the clusters, but their decay. These two processes can be distinguished if the dependence of the characteristic rate of the slow process Γ_2 on the scattering vector q is available: according to Uzgiris and Golibersuch (63),

$$\Gamma_2 = \Gamma_0 + D_2 q^2, \tag{17}$$

where Γ_0 is the rate of cluster decay, whose contribution to Γ_2 does not depend on the scattering vector q, and D_2 is the cluster diffusion coefficient.

The two limiting cases of Eq. 17 are $\Gamma_0 \gg D_2 q^2$, and $\Gamma_0 \ll D_2 q^2$. In the first case, $\Gamma_2 = \Gamma_0$, Γ_2 does not depend on the scattering vector, i.e., on the scattering angle, and the characteristic time of the slow process in Figs. 1 *b* and 6 is in fact the cluster lifetime. In the second case, $\Gamma_2 = D_2 q^2$, the slow process in Figs. 1 *b* and 6 is the cluster diffusion, and the cluster lifetime is longer than the characteristic diffusion time τ_2. The strong absorbance of Hb solutions at all visible wavelengths prevents the analyses of the angular dependence of Γ_2. Approximate determinations at scattering angles of 30°, 60°, and 90° revealed that Γ_2 is a strong function of the scattering vector. Thus, determinations of the cluster sizes R_2 using Eq. 4 and assuming that $\Gamma_2 = D_2 q^2$ do not carry a significant bias. From the inequality $\Gamma_0 \ll D_2 q^2$ with $q^2 = 3.5 \times 10^{10}$ cm^{-2} and $D_2 = 2 \times 10^{-9}$ cm^{2}s^{-1}, $\Gamma_0 \ll 70$ s^{-1}, and the cluster lifetimes have a lower bound $1/\Gamma_0 \approx 15$ ms.

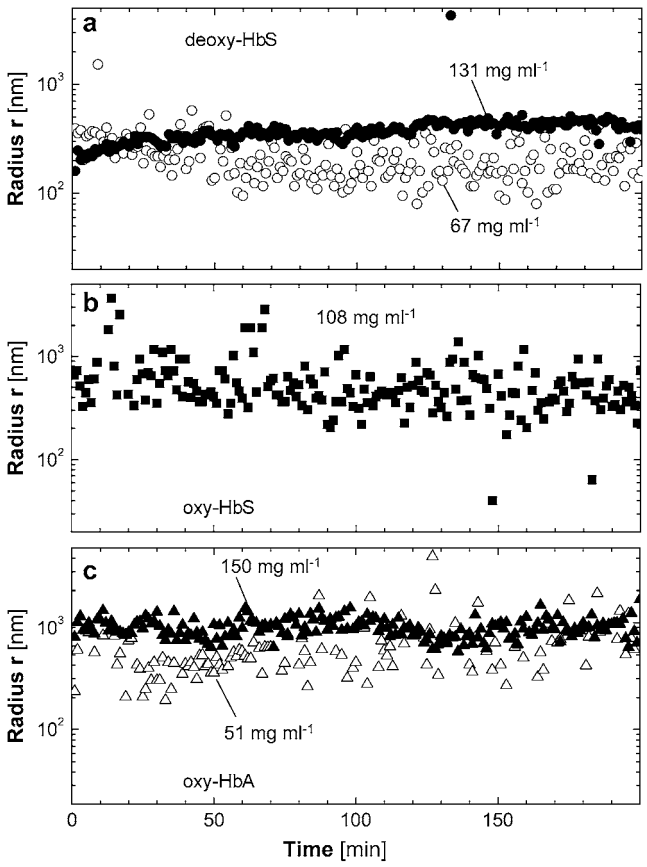

FIGURE 7 Time dependence of the radii of dense liquid clusters in solutions of the three hemoglobin variants as indicated in the plots, at the concentrations shown, at 25°C.

Dependence of clusters radii and number density of temperature and Hb concentration

The temperature dependencies of the radii R_2, number densities n_2, and volume fractions occupied by the clusters ϕ_2 for the three Hb variants are shown in Fig. 8. All data points in this figure are the averages of the respective variables determined every 60 s over 3 h, as in the traces in Fig. 7. For deoxy-HbS, R_2 is nearly independent of temperature. The number density of the clusters is relatively steady, and the volume fraction ϕ_2 increases from $\sim 10^{-3}$ at 10°C to significant $\sim 1\%$ at 30°C. Only small clusters, producing weak signal with a large error, were detected below 30°C at the tested concentration of oxy-HbS. At higher temperatures, the cluster size R_2 increases with temperature. The errors in the n_2 and ϕ_2 data for oxy-HbS at $T < 30$°C in Fig. 8 *c* are too high to plot, and even at $T > 30$°C, the data for ϕ_2 do not reveal a meaningful temperature trend. At $T > 30$°C, n_2 for oxy-HbS decreases with temperature. For oxy-HbA, R_2 and n_2 are nearly steady with temperature. Again, the accumulation of errors in the determination of ϕ_2 does not allow a conclusion about variations of ϕ_2 with temperature.

Fig. 9 shows the dependencies of the cluster radii R_2 and volume fractions ϕ_2 for the three Hb variants on the Hb concentration of the solution in which clusters form. For deoxy HbS and oxy-HbA, both R_2 and ϕ_2 increase as Hb concentration is increased. This seems to be the expected

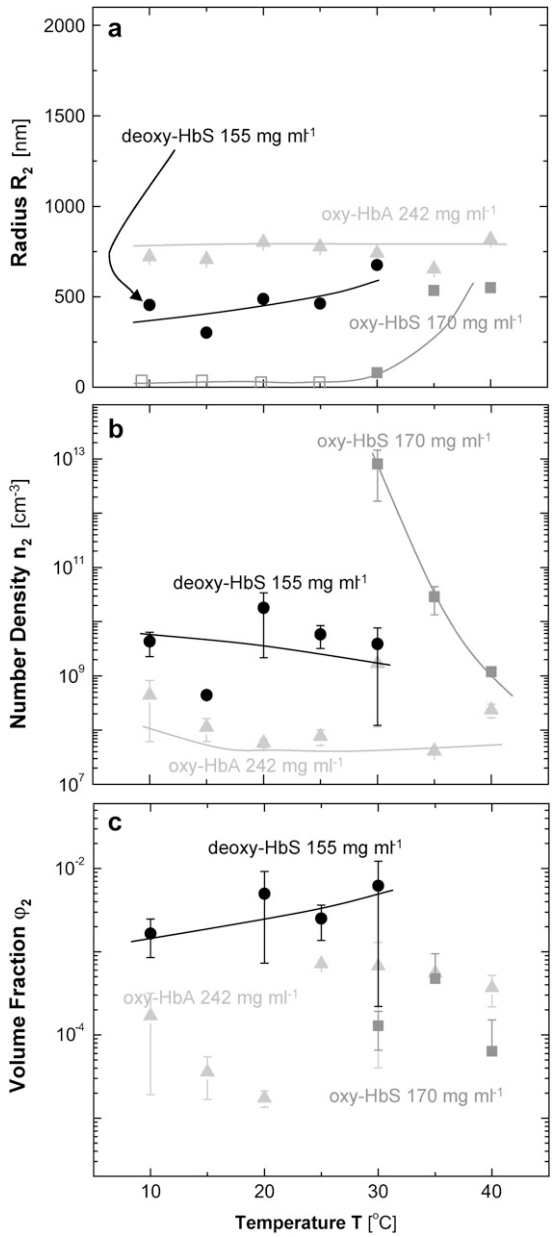

FIGURE 8 Dependencies of the radii of the dense liquid clusters R_2 in *a*, their number densities n_2 in *b*, and the fractions of the total solution volume ϕ_2 occupied by them in *c* on temperature T for the three hemoglobin variants as indicated in the plots, for the concentrations shown in the plots. Each data point is the average of a trace similar to those in Fig. 7. Error bars represent 95% confidence intervals of these averages and are smaller than symbol size in *a*. Solid lines are just guides for the eye. For oxy-HbS below 30°C, the A_2/A_1 ratios are 0.02–0.04, i.e., the determinations of R_2 have errors ~40% (see Fig. 4 and Eq. 4) and are denoted with open symbols. The corresponding data for n_2 and ϕ_2 (see Eq. 14) have significantly higher errors and are not shown in *b* and *c*.

behavior—higher Hb concentration in the solution leads to stronger driving force for cluster formation. Quite surprisingly, the clusters for oxy-HbS decrease in size and volume fraction, and at $C_{\text{oxy-HbS}} > 150$ mg ml^{-1}, no clusters are observed.

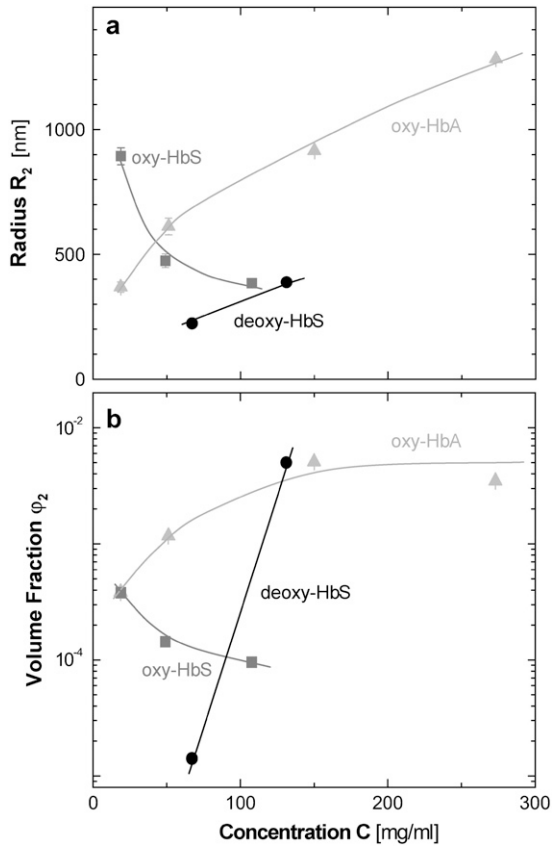

FIGURE 9 Dependencies of the radii of the dense liquid clusters R_2 and the fractions of the total solution volume ϕ_2 occupied by them on the concentration of each respective Hb variant as indicated in the plots at 25°C. Each data point in the average of a trace is similar to those in Fig. 7. Error bars represent intervals of 95% confidence of these averages and are comparable to symbol size in both *a* and *b*. Solid lines are just guides for the eye. No clusters of oxy-HbS are detected at this temperature in solutions of concentration higher than 100 mg ml^{-1}.

DISCUSSION

The nature of the clusters

As discussed in the Introduction, the only macroscopic phases in oxy-HbS and oxy-HbA are crystals. In addition to these, in deoxy-HbS solutions polymers may form, which over long times transform to crystals. The discussion below focuses on deoxy-HbS solutions; however, all observations and conclusions, which do not involve polymer formation, including those on the dense liquid, are valid also for oxy-HbS and oxy-HbA. The similarity suggests that the mutation from glutamate to valine in HbS, which allows a directional and relatively short-range hydrophobic contacts between HbS molecules, does not affect the clustering behavior. Thus, the formation of the dense liquid clusters is due to long-range forces, which are similar for the three Hb variants (24).

The observations on the deoxy-HbS polymers and crystals indicate that at concentrations higher than the respective solubility, the free energies ΔG of the polymers and crystals are lower than ΔG of the solution, and ΔG of the crystals

is lower than that of the polymers. The free energy landscape (64) of these three phases is schematically depicted in Fig. 10. The abscissa in the diagram in Fig. 10 is a one-dimensional projection of the full set of order parameters characterizing the phases in the hemoglobin + solvent system. This coordinate can be approximately thought of as HbS density + degree of ordering of the HbS molecules. We depict on the same diagram all other phases plausible in a deoxy-HbS solution: disordered aggregates, dense liquid, and loose network of molecules. The density and degree of ordering of these phases are between those for the HbS solution and the polymers; however, the relative location of each of these three phases along the configuration coordinate axis might be different from the one shown in Fig. 10. Since neither of these phases has been observed to occupy macroscopic spaces in a near-physiological deoxy-HbS solution, either continuous or discontinuous, their free energies must be higher than those of the solution, as depicted in Fig. 10.

It was shown that increasing the concentration of the phosphate buffer of the deoxy-HbS solution, or adding polyethylene glycol, leads to the formation of macroscopic dense liquid (30,35–37). In terms of the diagram in Fig. 10, these two effectors lower the free energy of the dense liquid to a level below the one of the deoxy-HbS solution.

The clusters could consist of any of the condensed phases in Fig. 10. In Results above, we showed that these are indeed clusters diffusing in the solution and not loose networks encompassing large solution volumes. To exclude the crystals as material for the clusters, we note that the clusters form within several seconds after solution preparation, which is faster by many orders of magnitude than the crystal nucleation times. Furthermore, for deoxy-HbS, both tested concentrations are below the polymer solubility, hence, these are not short HbS fibers. The fast appearance after solution preparation and the significant intensity scattered from them (compare A_2 and A_1 in Figs. 1 and 6) indicate that these clusters are not pieces of a loose network of Hb molecules. In contrast, clusters of dense liquid could exhibit any of the observed behaviors: extremely fast formation of 1–2 μm in size dense liquid droplets has been observed with the protein lysozyme (65), fast formation and decay of mesoscopic clusters has been recorded with the protein lumazine synthase (66). Thus, we conclude that these are clusters of dense liquid of the respective Hb variant.

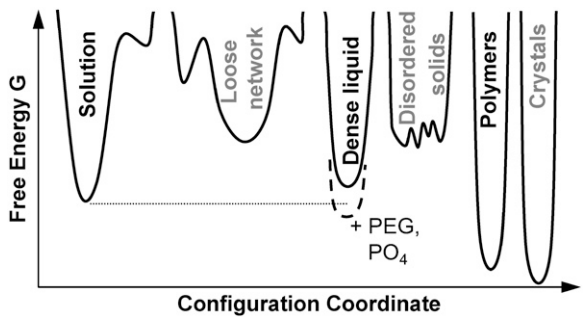

FIGURE 10 Free energy G landscape for different phases possible in deoxy-HbS solutions.

According to the discussion above, the dense liquid has a higher free energy ΔG than the Hb solution under the tested near-physiological conditions. In support of this conclusion, we note that if the clusters were of a stable phase, their size would increase in time, in contrast to the observation of a steady size in Fig. 7. Indeed, tests with the proteins insulin and lumazine synthase under condition in which crystals are stable demonstrate that the formation of a stable phase proceeds with an induction time. After this time, the characteristic size of the new-phase formations increases monotonically in time until it becomes bigger than the light scattering detection limit of a few micrometers.

The cluster lifetimes with a lower bound of 15 ms allow us to decide if the clusters are metastable or unstable with respect to the Hb solutions. These lifetimes are macroscopic and orders of magnitude longer than the characteristic molecular times of 10^{-12}–10^{-14} s. This estimate suggests that the cluster decay is delayed by a free energy barrier, i.e., the clusters are metastable and not unstable (i.e., not mere fluctuations of Hb concentration) with respect to the Hb solutions, as depicted in Fig. 10.

Microscopic model of clusters

The only microscopic model of cluster formation explains their finite size with the balance of intermolecular attraction, due to van der Waals, hydrophobic, or other forces, and repulsion between like-charged species (67). The main result of this theory is that large clusters could be expected only if the electrostatic repulsive energy is high. Thus, clusters of more than 100 molecules require repulsive energies of the order of $10^4\ k_BT$ (67). This theory has been found to adequately describe the existence of clusters of a few tens of particles or molecules in colloid suspensions (68–70) and in solutions of the protein lysozyme at low ionic strength (70). This theory is certainly inapplicable to the clusters of the hemoglobin variants discussed above: with sizes of several hundred nanometers, they likely contain an order of 10^6 molecules. If these clusters form according to the mechanism put forth in Sciortino et al. (67), they would require a strong electrostatic repulsion, which is hard to envision for the almost neutral Hb molecules under near-physiological pH. Indeed, the isoionic pH for HbA is 6.8 (62) and slightly higher for HbS, and the R-to-T transition has a minor effect on this value. Thus at the working pH = 7.35, the Hb molecules carry $\sim$1 negative charge. If the Hb molecules attain charge after they enter the clusters, the high level of electrostatic energy required for clusters as large as those observed would drive apart different parts of the Hb molecule and denature the molecules (V. Lubchenko, University of Houston, private communication, 2006).

At this point, there exists no microscopic theory that could explain at the molecular level the mechanism of cluster stability, and the factors that determine their lifetimes and

sizes. The properties of the clusters discussed here can serve as the basis for the formulation of such a theory. Particularly illuminating appears the observation in Fig. 9 that whereas the sizes and volume fractions of the deoxy-HbS and oxy-HbA clusters increase at higher hemoglobin concentrations, those characteristics for oxy-HbS decrease. The counterintuitive behavior of oxy-HbS suggests that the cluster mechanism cannot be understood by focusing on the intermolecular interactions in the solution: as discussed in Results, the solution thermodynamics readily explain only the behavior of the deoxy-HbS and oxy-HbA clusters. It is likely that the disappearance of the oxy-HbS clusters at higher Hb concentrations is due to a change of the cluster properties, which lowers the cluster stability.

Clusters and nucleation

In another study (O. Galkin, W. Pan, L. Filobelo, R. E. Hirsch, R. L. Nagel, and P. G. Vekilov, unpublished), we show that the nucleation of deoxy-HbS polymers proceeds via a two-step mechanism, i.e., the nuclei of the polymer fibers form inside the clusters discussed here. Even more importantly, the results in Galkin et al. (O. Galkin, W. Pan, L. Filobelo, R. E. Hirsch, R. L. Nagel, and P. G. Vekilov, unpublished) show that the rate of nucleation of the HbS polymers is limited by the rate of formation of the clusters. This is because in contrast to nucleation of crystals, the nucleation of HbS polymers is very fast and occurs over timescales of a few seconds. Thus, by controlling the stability and the rate of formation of the clusters, one can control the rate of HbS polymer nucleation. The results with addition of polyethylene glycol and increase of phosphate concentration (30,35–37) show that the stability of the dense liquid is strongly affected by the solution composition. The nature of additives that affect the stability of the dense liquid requires detailed further studies. Still, these considerations lead to a very significant conclusion: the presence of clusters and their role in the HbS polymer nucleation provide a new handle for control of the nucleation process. The previous outlook on HbS polymer nucleation via a direct classical-type mechanism (34) allows for a single control parameter at fixed temperature: the deoxy-HbS activity. The realization that other solution components may have strong effects on the nucleation rate, and that these effects would occur through the volume fraction occupied by dense liquid clusters, offers two novel insights: i), that much of the variability of the clinical manifestations of sickle cell anemia may be due to the numerous nonprotein components of the red blood cell cytosol, and ii), that a treatment could be sought among these components or among other compounds which would penetrate the red cells and delay the polymerization kinetics by lowering the cluster concentration.

We thank Panagiotis Katsonis for help with the result interpretation, Vassiliy Lubchenko for insightful discussions on the nature of clusters in protein solutions and for numerous suggestions on the manuscript, and Veselina Uzunova for critical reading of the manuscript.

This work was supported by the National Heart, Lung, and Blood Institute (National Institutes of Health) through Grant G091474.

REFERENCES

1. Pauling, L., H. A. Itano, S. J. Singer, and I. C. Wells. 1949. Sickle cell anemia, a molecular disease. *Science.* 111:543–548.
2. Ingram, V. M. 1956. A specific chemical difference between the globins of normal human and sickle cell anaemia haemoglobin. *Nature.* 178:792–794.
3. Ingram, V. M. 1959. Abnormal human haemoglobins. III. The chemical difference between normal and sickle cell haemoglobins. *Biochim. Biophys. Acta.* 36:402–411.
4. Perutz, M. F. 1976. Structure and mechanism of haemoglobin. *Br. Med. Bull.* 32:195–208.
5. Wishner, B., K. Ward, E. Lattman, and W. Love. 1975. Crystal structure of sickle-cell deoxyhemoglobin at 5 A resolution. *J. Mol. Biol.* 98:179–194.
6. Fronticelli, C., and R. Gold. 1976. Conformational relevance of the beta6Glu replaced by Val mutation in the beta subunits and in the beta(1–55) and beta(1–30) peptides of hemoglobin S. *J. Biol. Chem.* 251:4968–4972.
7. Dykes, G. W., R. H. Crepeay, and S. J. Edelstein. 1979. Three dimensional reconstruction of 14-filament fibers of hemoglobin S. *J. Mol. Biol.* 130:451–472.
8. Carrager, B., D. A. Bluemke, B. Gabriel, M. J. Potel, and R. Josephs. 1988. Structural analysis of polymers of sickle cell hemoglobin. I. Sickle cell hemoglobin fibers. *J. Mol. Biol.* 199:315–331.
9. Briehl, R. W. 1995. Nucleation, fiber growth and melting and domain formation and structure in sickle cell hemoglobin gels. *J. Mol. Biol.* 245:710–723.
10. Noguchi, C. T., and A. N. Schechter. 1981. The intracellular polymerization of sickle hemoglobin and its relevance to sickle cell disease. *Blood.* 58:1057–1069.
11. Briehl, R. W. 1983. Rheology of hemoglobin S gels: possible correlation with impaired microvascular circulation. *Am. J. Ped. Hem. Onc.* 5:390–398.
12. Nishio, I., T. Tanak, S.-T. Sun, Y. Imanishi, and S. T. Ohnishi. 1983. Hemoglobin aggregation in single red blood cells of sickle cell anemia. *Science.* 220:1173–1175.
13. Brirtenham, G. M., A. N. Schechter, and C. T. Noguchi. 1985. Hemoglobin S polymerization: primary determinant in the hemolytic and clinical severity of the sickling syndromes. *Blood.* 65:183–201.
14. Eaton, W. A., and J. Hofrichter. 1987. Hemoglobin S gelation and sickle cell disease. *Blood.* 70:1245–1266.
15. Mozzarelli, A., J. Hofrichter, and W. A. Eaton. 1987. Delay time in hemoglobin S polymerization prevents most of the cells from sickling in vivo. *Science.* 237:500–506.
16. Minton, A. P. 1977. Non-ideality and the thermodynamics of sickle cell hemoglobin gelation. *J. Mol. Biol.* 110:89–103.
17. Ross, P. D., and A. P. Minton. 1977. Analysis of non-ideal behavior in concentrated hemoglobin solutions. *J. Mol. Biol.* 112:437–452.
18. Lunelli, L., E. Bucci, and G. Baldini. 1993. Electrostatic Interactions in hemoglobin from light scattering experiments. *Phys. Rev. Lett.* 70:513–516.
19. Antosiewicz, J., and D. Porschke. 1995. Electrostatics of hemoglobins from measurements of the electric dichroism and computer simulations. *Biophys. J.* 68:655–664.
20. Berreta, S., G. Chirico, D. Arosio, and G. Baldini. 1997. Role of ionic strength on hemoglobin interparticle interactions and subunit dissociation from light scattering. *Macromolecules.* 30:7849–7855.
21. Berreta, S., G. Chirico, D. Arosio, and G. Baldini. 1997. Photon correlation spectroscopy of interacting and dissociating hemoglobin. *J. Chem. Phys.* 106:8427–8435.
22. Han, J., and J. Herzfeld. 1998. Interpretation of the osmotic behavior of sickle cell hemoglobin solutions: different interactions among monomers and polymers. *Biopolymers.* 45:299–306.

23. Ivanova, M., R. Jasuja, S. Kwong, R. W. Briehl, and F. A. Ferrone. 2000. Non-ideality and the nucleation of sickle hemoglobin. *Biophys. J.* 79:1016–1022.
24. Vekilov, P. G., A. R. Feeling-Taylor, D. N. Petsev, O. Galkin, R. L. Nagel, and R. E. Hirsch. 2002. Intermolecular interactions, nucleation and thermodynamics of crystallization of hemoglobin C. *Biophys. J.* 83:1147–1156.
25. Ferrone, F. A., and M. A. Rotter. 2004. Crowding and the polymerization of sickle hemoglobin. *J. Mol. Recognit.* 17:497–504.
26. Corbett, J. D., W. E. Mickols, and M. F. Maestre. 1995. Effect of hemoglobin concentration on nucleation and polymer formation in sickle red blood cells. *J. Biol. Chem.* 270:2708–2715.
27. Cao, Z., and F. A. Ferrone. 1996. A 50th order reaction predicted and observed for sickle hemoglobin nucleation. *J. Mol. Biol.* 256:219–222.
28. Liao, D., J. J. Martin de Llano, J. P. Himanen, J. M. Manning, and F. A. Ferrone. 1996. Solubility of sickle hemoglobin measured by a kinetic micromethod. *Biophys. J.* 70:2442–2447.
29. Louderback, J. G., S. K. Ballas, and D. B. Kim-Shapiro. 1999. Sickle hemoglobin polymer melting at high concentration phosphate buffer. *Biophys. J.* 76:2216–2222.
30. Galkin, O., K. Chen, R. L. Nagel, R. E. Hirsch, and P. G. Vekilov. 2002. Liquid-liquid separation in solutions of normal and sickle cell hemoglobin. *Proc. Natl. Acad. Sci. USA.* 99:8479–8483.
31. Galkin, O., and P. G. Vekilov. 2004. Mechanisms of homogeneous nucleation of polymers of sickle cell anemia hemoglobin in deoxy state. *J. Mol. Biol.* 336:43–59.
32. Adachi, K., and T. Asakura. 1981. Aggregation and crystallization of hemoglobins A, S, and C. Probable formation of different nuclei for gelation and crystallization. *J. Biol. Chem.* 256:1824–1830.
33. Makinen, M. W., and C. W. Sigountos. 1984. Structural basis and dynamics of the fiber-to-crystal transition of sickle cell hemoglobin. *J. Mol. Biol.* 178:439–476.
34. Eaton, W. A., and J. Hofrichter. 1990. Sickle cell hemoglobin polymerization. *In* Advances in Protein Chemistry. C. B. Anfinsen, J. T. Edsal, F. M. Richards, and D. S. Eisenberg, editors. Academic Press, San Diego. 63–279.
35. Serrano, M. D., O. Galkin, S.-T. Yau, B. R. Thomas, R. L. Nagel, R. E. Hirsch, and P. G. Vekilov. 2001. Are protein crystallization mechanisms relevant to understanding and control of polymerization of deoxyhemoglobin S? *J. Cryst. Growth.* 232:368–375.
36. Chen, K., S. K. Ballas, R. R. Hantgan, and D. B. Kim-Shapiro. 2004. Aggregation of normal and sickle hemoglobin in high concentration phosphate buffer. *Biophys. J.* 84:4113–4121.
37. Chen, Q., P. G. Vekilov, R. L. Nagel, and R. E. Hirsch. 2004. Liquid-liquid separation in hemoglobins: distinct aggregation mechanisms of the β6 mutants. *Biophys. J.* 86:1702–1712.
38. ten Wolde, P. R., and D. Frenkel. 1997. Enhancement of protein crystal nucleation by critical density fluctuations. *Science.* 277:1975–1978.
39. Galkin, O., and P. G. Vekilov. 2000. Control of protein crystal nucleation around the metastable liquid-liquid phase boundary. *Proc. Natl. Acad. Sci. USA.* 97:6277–6281.
40. Lomakin, A., N. Asherie, and G. B. Benedek. 2003. Liquid-solid transition in nuclei of protein crystals. *Proc. Natl. Acad. Sci. USA.* 100: 10254–10257.
41. Vekilov, P. G. 2004. Dense liquid precursor for the nucleation of ordered solid phases from solution. *Cryst. Growth Des.* 4:671–685.
42. Garetz, B., J. Matic, and A. Myerson. 2002. Polarization switching of crystal structure in the nonphotochemical light-induced nucleation of supersaturated aqueous glycine solutions. *Phys. Rev. Lett.* 89:175501.
43. Oxtoby, D. W. 2002. Crystals in a flash. *Nature.* 420:277–278.
44. Pan, W., A. B. Kolomeisky, and P. G. Vekilov. 2005. Nucleation of ordered solid phases of protein via a disordered high-density state: phenomenological approach. *J. Chem. Phys.* 122:174905.
45. Kashchiev, D., P. G. Vekilov, and A. B. Kolomeisky. 2005. Kinetics of two-step nucleation of crystals. *J. Chem. Phys.* 122:244706.
46. Schmitz, K. S. 1990. Dynamic Light Scattering by Macromolecules. Academic Press, New York.
47. Eisenberg, D., and D. Crothers. 1979. Physical Chemistry with Applications to Life Sciences. Benjamin Cummings, Menlo Park, CA.
48. Berry, P. S., S. A. Rice, and J. Ross. 2000. Physical Chemistry. Oxford University Press, New York.
49. Schatzel, K. 1993. Single-photon correlation techniques. *In* Dynamic Light Scattering. The Method and Some Applications. W. Brown, editor. Clarendon Press, Oxford. 76–148.
50. Provencher, S. W. 1982. CONTIN: a general purpose constrained regularization program for inverting noisy linear algebraic and integral equations. *Comp. Phys. Communications.* 27:229–242.
51. Provencher, S. W. 1982. A constrained regularization method for inverting data represented by linear algebraic equations. *Comp. Phys. Communcations.* 27:213–227.
52. 2004. CRC Handbook on Chemistry and Physics: CRC Press, LLC.
53. Ross, P. D., and A. P. Minton. 1977. Hard quasi-spherical model for the viscosity of hemoglobin solutions. *Biochem. Biophys. Res. Commun.* 76:971–976.
54. Ford, N. C. 1972. Biochemical applications of laser Rayleigh-scattering. *Chem. Scr.* 2:193–196.
55. Chen, F. C., W. Tscharnuter, D. Schmidt, and B. Chu. 1974. Experimental evaluation of macromolecular polydispersity in intensity correlation spectroscopy using the cumulant expansion technique. *J. Chem. Phys.* 60:1675–1676.
56. Ross, P. D., J. Hofrichter, and W. A. Eaton. 1977. Thermodynamics of gelation of sickle cell deoxyhemoglobin. *J. Mol. Biol.* 115:111–134.
57. Huglin, M. B. 1962. Specific refractive index increments. *In* Light Scattering from Protein Solutions. M. B. Huglin, editor. Academic Press, New York. 165–331.
58. Peters, R. 1993. Noise on photon correlation functions and its effect on data reduction algorithms. *In* Dynamic Light Scattering. The Method and Some Applications. W. Brown, editor. Clarendon Press, Oxford. 149–176.
59. Stepanek, P. 1993. Data analysis in dynamic light scattering. *In* Dynamic Light Scattering. The Method and Some Applications. W. Brown, editor. Clarendon Press. 177–241.
60. Sohn, I. S., and R. Rajagopalana. 2004. Microrheology of model quasi-hard-sphere dispersions. *J. Rheol.* 48:117–142.
61. 2000–2001. Handbook of Chemistry and Physics, 81st ed. CRC Press, Boca Raton, FL.
62. Nelson, D. L., and M. M. Cox. 2000. Lehninger's Principles of Biochemistry, 3rd ed. W. H. Freeman, New York.
63. Uzgiris E. E., and D. C. Golibersuch. 1974. Excess scattered-light intensity fluctuations from hemoglobin. *Phys. Rev. Lett.* 32:37 37–40.
64. Frauenfelder, H., S. Sligar, and P. Wolynes. 1991. The energy landscapes and motions of proteins. *Science.* 254:1598–1603.
65. Shah, M., O. Galkin, and P. G. Vekilov. 2004. Smooth transition from metastability to instability in phase separating protein solutions. *J. Chem. Phys.* 121:7505–7512.
66. Gliko, O., N. Neumaier, W. Pan, I. Haase, M. Fischer, A. Bacher, S. Weinkauf, and P. G. Vekilov. 2005. A metastable prerequisite for the growth of lumazine synthase crystals. *J. Am. Chem. Soc.* 127:3433–3438.
67. Sciortino, F., S. Mossa, E. Zaccarelli, and P. Tartaglia. 2004. Equilibrium cluster phases and low-density arrested disordered states: the role of short-range attraction and long-range repulsion. *Phys. Rev. Lett.* 93:055701.
68. Liu, Y., W.-R. Chen, and S.-H. Chen. 2005. Cluster formation in two-Yukawa fluids. *J. Chem. Phys.* 122:044507.
69. Mossa, S., F. Sciortino, P. Tartaglia, and E. Zaccarelli. 2004. Ground-state clusters for short-range attractive and long-range repulsive potentials. *Langmuir.* 20:10756–10763.
70. Stradner, A., H. Sedgwick, F. Cardinaux, W. C. K. Poon, S. U. Egelhaaf, and P. Schurtenberger. 2004. Equilibrium cluster formation in concentrated protein solutions and colloids. *Nature.* 432:492–495.